tion of H. L. Davis in generating the first-principles band energies for nickel has been invaluable.

*Research sponsored by the U. S. Atomic Energy Commission under contract with Union Carbide Corp.

[1]G. Gilat and L. J. Raubenheimer, Phys. Rev. 144, 390 (1966).

[2]As far as we have been able to ascertain, Brust [Phys. Rev. 139, A489 (1965)] was the first to employ quadratic interpolation extensively for BZ integration.

[3]F. M. Mueller, J. W. Garland, M. H. Cohen, and K. H. Bennemann, Ann. Phys. (N.Y.) 67, 19 (1971).

[4]The idea of combining various interpolation schemes is, of course, not new. A combined linear-quadratic approach very similar in spirit to the one we use here was introduced by Janak; however, we were unaware of his work at the time we amalgamated the GR and Quad schemes. Descriptions of Janak's work are given in (a) J. F. Janak, Phys. Letters 28A, 570 (1969); (b) J. F. Janak, in *Computational Methods in Band Theory*, edited by P. M. Marcus, J. F. Janak, and A. R. Williams (Plenum, New York, 1971), p. 323.

[5]E. C. Svensson, B. N. Brockhouse, and J. M. Rowe, Phys. Rev. 155, 619 (1967); R. M. Nicklow, G. Gilat, H. G. Smith, L. J. Raubenheimer, and M. K. Wilkinson, Phys. Rev. 164, 922 (1967).

[6]J. S. Faulkner, H. L. Davis, and H. W. Joy, Phys. Rev. 161, 656 (1967); H. L. Davis, J. S. Faulkner, and H. W. Joy, Phys. Rev. 167, 601 (1968); H. L. Davis, in *Computational Methods in Band Theory*, edited by P. M. Marcus, J. F. Janak, and A. R. Williams (Plenum, New York, 1971), p. 183. Some readers may be interested in knowing that it took approximately 28 min of IBM 360/91 time to generate the KKR ($l_{max}=3$) energies at 916 k points.

[7]G. Gilat and F. Herman, Ann. Phys. (N. Y.) 67, 432 (1971).

PHYSICAL REVIEW B VOLUME 5, NUMBER 4 15 FEBRUARY 1972

Microwave Transmission Spectroscopy of Copper and Silver

T. G. Phillips, G. A. Baraff, and P. H. Schmidt
Bell Telephone Laboratories, Murray Hill, New Jersey 07974
(Received 25 August 1971)

This paper describes a set of microwave transmission experiments carried out at a frequency of 35 GHz and a temperature of 4.2 K, in the presence of a dc magnetic field applied normal to the plane of the sample. Strong resonant bursts of transmission are observed in samples thin compared with the mean free path and these are shown to be a new form of cyclotron resonance, not of the Azbel-Kaner type. These resonances are called "cyclotron phase resonances," because they occur when many propagating electrons arrive at the second surface of the sample with the same microwave phase. This resonant effect arises where there is a large region of constant mass on the Fermi surface. In thick samples, a high-frequency version of the Gantmakher-Kaner oscillation is observed. A mechanism is proposed, to explain the propagation in thick samples, which is concerned with the "topological effectiveness" of the electron orbits. A measurement of the microwave phase of the oscillation is used to determine the Fermi velocity by a time-of-flight technique.

I. INTRODUCTION

A thick slab of metal is generally thought of as nontransparent to microwave-frequency electromagnetic radiation when its thickness is much greater than the skin depth δ. However, there are conditions under which an electromagnetic wave initiated at one surface may be detected at the second. Various mechanisms which are known to exist for such effects include conduction-electron propagation (anomalous-field penetration),[1] plasma-wave propagation,[2] spin diffusion,[3] spin-wave propagation,[4] and antiresonance transparency[5] in magnetic metals. Other possible mechanisms would presumably include helicon waves (or Alfvén waves) at high fields and phonons in superconductors.

This paper discusses both experimentally and theoretically some aspects of the mechanism of electromagnetic-wave propagation associated with conduction electrons of long mean free path, at microwave frequencies, and in the geometry of a dc magnetic field normal to the plane of the surface of the specimen. Generically, the phenomena we shall be studying would be classified as types of anomalous-field penetration,[1] by which it is meant that the dynamics of transmission is dominated by the trajectories of individual electrons in the magnetic field rather than by the collective aspects of the self-consistent fields to which the motion of these electrons give rise. However, the specific aspects of anomalous-field penetration which will concern us here have only recently been observed and understood,[6,7] and the present work is a full exposition of the ideas and observations of our earlier commu-

nications.

The experiment we are concerned with is a microwave transmission measurement in which microwave radiation is directed at one face of a slab of single-crystal pure metal. At the second surface, the phase and amplitude of the signal transmitted through the sample are measured as a function of the dc magnetic field surrounding and permeating the sample. Such a transmission spectrum shows considerable structure, whose identification concerns us here.

Several novel results are found in specimens of copper and silver at liquid-helium temperatures, including a method for direct time-of-flight measurement of Fermi velocities, a new type of anomalous-field propagation, and the observation of a set of strong transmission resonances which we describe as "cyclotron phase resonance."

The problem of the propagation of electromagnetic radiation through metallic sheets (ignoring the electron spin) in the anomalous-skin-effect region, when a dc magnetic field is normal to the sheet, has been formulated in a self-consistent manner by Gantmakher and Kaner[8] in the limit that the incident radiation frequency is negligible compared with the electron cyclotron frequency. This was formally extended to arbitrary frequency by Naberezhnyk and Dan'shin.[9] We, however, take a simplified point of view which implies a division of the electric field in the metal into two regions. One is near the surface where the field is rapidly damped (skin depth), and the second extends to a depth of the order of the electron mean free path, where the field is much more slowly damped. This point of view was earlier put forward by Weisbuch and Libchaber.[10] Fields in the skin depth can now be thought of as transverse driving fields which give transverse momentum to those electrons traveling across the sample (the ineffective electrons in the Pippard sense). Both the low-frequency Gantmakher-Kaner[8] analysis and the simplified point of view lead to the prediction of an oscillatory phase for a component of the transmitted field as a function of dc magnetic field strength and such oscillations [Gantmakher-Kaner oscillations (GKO)] have been observed for various metals. We may view these oscillations as resulting from the sum of electromagnetic fields at the receiving surface of the sheet due to individual conduction electrons propagating along helixes under the action of the normal dc magnetic field H. The wave vector associated with such a helix is given by

$$2\pi/u = \omega_c/\overline{V}_H \,, \tag{1.1}$$

where u is the pitch of the helix, ω_c is the cyclotron frequency, and $\overline{V}_H$ is the electron average orbit velocity normal to the sheet, for some particular value of the Fermi wave vector k_H. The phase of the transmitted field, referred to that of the driving field, depends upon the rotation that the electron has suffered on reaching the second surface. This phase varies as the pitch of the helix varies with the magnetic field. Of course the transmitted field is the result of summing over all electrons on the Fermi surface which have sufficient free path to reach the second surface, and the phases of the various fields tend to cancel. The weak transmitted signal (GKO) results from a breakdown of the cancellation, for instance, due to a stationary value of the pitch of the helix u as a function of position on the Fermi surface k_H. The period of these oscillations gives information about the parameters of the Fermi surface.

At microwave frequencies the arguments must be reconsidered, since for typical values of laboratory magnetic fields the driving frequency ω is comparable with the cyclotron frequencies of the Fermi-surface electrons. Now in time t, in which the electron rotates on its helix through a phase angle $\omega_c t$, the driving field rotates an angle ωt resulting in a change in the helix length, and Eq. (1.1) becomes

$$2\pi/u = (\omega \pm \omega_c)/\overline{V}_H \,, \tag{1.2}$$

where the $\pm$ sign refers to the two possible senses of polarization. The phase of the transmitted field with respect to the driving field is now given by

$$\varphi_L = \varphi_\delta + (\omega \pm \omega_c)L/\overline{V}_H \,, \tag{1.3}$$

where L is the specimen thickness and φ_δ is a phase shift introduced in the skin depth, but which is not a function of k_H.

An immediate consequence of expressions (1.2) and (1.3) is that, for the case of the negative sense of polarization, the pitch of the helix becomes infinite at $\omega = \omega_c$, and all electrons at the Fermi surface with that particular value of cyclotron frequency will be in phase with one another at the second surface. If the Fermi surface has significant regions of constant cyclotron frequency (or mass), powerful transmitted signals of a resonant character can be observed. We have termed this effect cyclotron phase resonance. As we shall show in this paper, copper and silver provide excellent examples of this effect, harmonics as well as fundamental resonances being clearly observable. This effect is particularly strong for copper where we identify the signals as being due to the large region of nearly constant mass between the belly and the necks.

A second important consequence of the high driving frequency is that the time of flight of an unscattered electron across a typical sample (of thickness, say, 10^{-1}–10^{-2} cm) is comparable with a cycle of the driving field. Thus if we can measure the absolute phase difference between the trans-

mitted and driving fields [Eq. (1.3)], for zero magnetic field on the specimen, we have measured the time of flight across the sample and thus the Fermi velocity. We describe such an experimental measurement for a particular group of electrons in copper in Sec. V.

A third consequence of the finite frequency of the experiment is that the information obtained about the Fermi surface from the GKO periods can now be a function of frequency. The condition that the pitch of the helix be stationary, as a function of k_H, is still appropriate, but the pitch is now frequency dependent, Eq. (1.2). Thus within limits the region of the Fermi surface giving rise to the GKO can be varied by changing the experimental frequency.

The metals copper and silver have been chosen for this investigation partly because they can be manufactured as high-purity single crystal, and partly because the Fermi surface is well known from previous investigations. We have used the results of Halse[11] to calculate orbit parameters as a function of k_H in order to compare with experiments and this calculation is described in Sec. III.

II. THEORY

A. Form of Transmitted Fields

The problem of electromagnetic-wave transmission through a high-conductivity metal in the anomalous-skin-effect regime has been considered by several authors.[8,9,12–16] In essence, the problem is simply stated: Perform a self-consistent calculation in which Maxwell's equations describe the fields resulting from a given current distribution, while the currents resulting from a given field distribution are to be calculated using a nonlocal conductivity, whose form is ultimately governed by the trajectories of the electrons. The nature of the trajectories is determined primarily by three factors, the details of the Fermi surface, the strength and orientation of the uniform static magnetic field (if present), and the fate of those electrons which collide with the surface of the sample.

Performing these calculations with sufficient attention to numerical detail to ensure that the results describe copper, say, or silver, would be exceedingly difficult. In addition to this practical difficulty, there is, concealed here, a fundamental conceptual difficulty, concerning the proper treatment of those electrons which collide with the surface of the sample. One does not really know how to describe the effect of their collisions with the surface, and yet one is sure[14] that certain features of the calculated fields will depend on how the electron-surface collisions are described.

In such a situation, a simpler approach is called for. The approach we choose comes closer to being able to account for our observations than does any

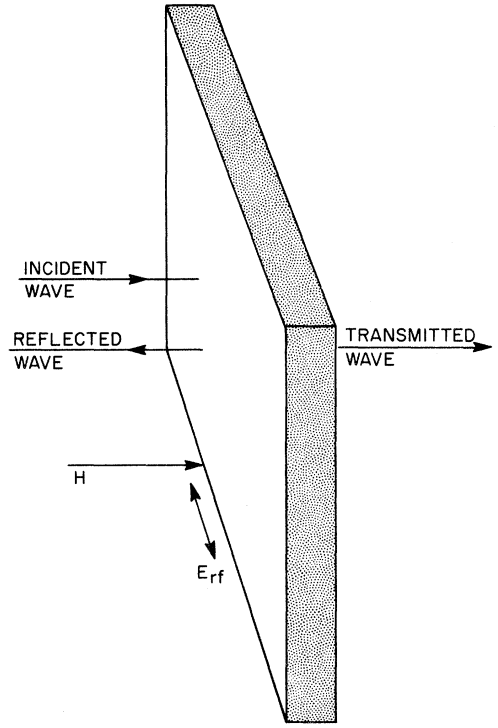

FIG. 1. Transmission scheme, showing incident, reflected, and transmitted waves.

of the calculations in which self-consistency is stressed but in which the true difficulty at the surfaces is either ignored or dismissed after a superficial discussion.

We consider a transmission experiment, as in Fig. 1. The incident transverse microwave field, of time dependence $e^{-i\omega t}$ (which we suppress throughout), is almost totally reflected from the metal slab and the small amount of field which does enter the slab decays almost to zero within a very short distance, the anomalous skin depth. We assume (and one is free to argue about how or whether these assumptions can be shown to follow from a proper treatment of the self-consistent-field problem) that under the conditions of our experiments the following are true:

(i) The transmitted field $\vec{e}^T$ is proportional to the current $\vec{j}$ at the emergent face of the slab:

$$e_\alpha^T = \sum_{\beta=x,y} M_{\alpha\beta} j_\beta(L) \ .$$

(ii) The current $\vec{j}(z)$ is related to the electric field in the slab via a nonlocal conductivity tensor σ:

$$j_\alpha(z) = \sum_{\beta=x,y} \int_0^L \sigma_{\alpha\beta}(z,z')\, e_\beta(z')\, dz' \ .$$

(iii) The electric field has appreciable amplitude only in the anomalous skin depth, a length which is very small compared to all other characteristic

lengths in the problem. Further, only the fact that the electric field is confined to the skin depth is important, and its internal structure within the skin depth plays no role. That is, we shall take

$$e_\alpha(z) = E_\alpha \delta(z) \ .$$

(iv) For the purposes of evaluating (2.1) below, we also assume that σ can be computed as though the slab were infinitely thick, ignoring the presence of the boundaries at $z=0$ and $z=L$. In this case, σ can depend only on the distance between z', the field plane, and z, the current plane. Combining these four assumptions gives us

$$e_\alpha^T = \sum_{\substack{\beta=x,y \\ \gamma=x,y}} M_{\alpha\beta}\, \sigma_{\beta\gamma}(L)\, E_\gamma \ . \tag{2.1}$$

(v) Although there is the possibility that M and E depend on ω, the frequency of the driving field, and on H, the strength of the magnetic field, we shall assume that such dependence is weak enough to be ignored.

These five assumptions, combined into Eq. (2.1), provide the theoretical framework within which our results may be understood. We shall base the entire analysis of this paper on Eq. (2.1). The concept here, essentially the same as that stated by Weisbuch and Libchaber,[10] is that the transmission is to be considered in two parts. First, the incident field is confined to the region near the face of the material by shielding currents which arise in a self-consistent way and which are governed by the short-range behavior of the conductivity. Next, this spatially confined field, which exists only in the skin depth, imparts transverse momentum to those other ("ineffective") electrons whose motion across the slab is governed by the long-range part of the conductivity.

Let us turn now to the evaluation of (2.1). First, note that for systems with threefold or greater rotational symmetry about the z axis, as will be the case here, the result of operating with the matrix M can be at most a multiplication by a constant followed by a rotation through some fixed angle about the z axis. Neither of these effects will play any role in our discussion so we ignore them both at the outset, replacing M by the unit matrix. Next, note that the calculation of the infinite medium nonlocal conductivity is usually carried out for monochromatic electric fields at frequency ω having the spatial form e^{-iqz}. From the resulting conductivity, designated as $\sigma(q,\omega)$, one obtains the nonlocal conductivity via a Fourier transform. Hence, Eq. (2.1), the formula we shall use for evaluating the transmitted fields, becomes

$$e_\alpha^T \approx \sum_\beta \int_{-\infty}^{\infty} dq\, \sigma_{\alpha\beta}(q,\omega)\, E_\beta\, e^{iqL} \ . \tag{2.2}$$

For a general Fermi surface, we may use the expression for the infinite medium conductivity given by Overhauser and Rodriguez,[17] namely,

$$\sigma_{\alpha\beta}(q,\omega) = \frac{4\pi e^2/i}{(2\pi\hbar)^3} \times \sum_{n=-\infty}^{+\infty} \int dk_H \, \frac{m^*(k_H)\, V_n^\alpha(q,k_H)\, V_n^\beta(q,k_H)^*}{q\bar{V}_H(k_H) - \omega - i\gamma - n\omega_c(k_H)} \ , \tag{2.3}$$

where k_H is the quasimomentum along the magnetic field direction, m^* is the cyclotron mass for electrons whose orbit (momentum space) lies in the plane at k_H, V_n^α are essentially Fourier coefficients of the transverse velocity components, $\bar{V}_H$ is the average velocity along the magnetic field for electrons at k_H, γ is a phenomenological electron-scattering frequency which is assumed to be the same for all electrons on the Fermi surface, and ω_c is the cyclotron frequency of electrons at k_H,

$$\omega_c(k_H) = eH/m^*(k_H)c \ . \tag{2.4}$$

The quantities m^*, V_n^α, and $\bar{V}_H$ depend on the details of the Fermi surface and involve integration of various functions of $\vec{k}$ around the orbit at k_H. Equation (2.3) expresses the conductivity as an integral over the various orbits (each at a fixed k_H) which electrons trace out in momentum space.

It will be exceedingly useful for us to approximate the $V_n^\alpha(q,k_H)$ coefficients by $V_n^\alpha(k_H)$, their value at $q=0$. [The $V_n^\alpha(k_H)$ are truly the Fourier coefficients of the transverse velocity components.] The justification for this step is simple to supply numerically for the electrons we shall be concerned with, but it is more instructive to qualitatively examine the electron motion. As an electron moves through the metal, its velocity in the z direction fluctuates about its average value $\bar{V}_H(k_H)$, and hence its position $z(t)$ oscillates about the position it would have had, $z^0(t)$, if its velocity had been the constant $\bar{V}_H$. Since it is moving through an electric field of the form e^{-iqz}, the phase of field it experiences also fluctuates about the value it would have experienced had its velocity been $\bar{V}_H$. This introduces the q dependence into $V_n^\alpha(q,k_H)$. If the wavelength of the field is long compared to the spatial excursion the electron makes about $z^0(t)$, then the phase fluctuations the electron experiences will be small. $V_n^\alpha(q,k_H)$ will then be essentially equal to its value for an electric field of infinite wavelength, i.e., equal to $V_n^\alpha(0,k_H)$.

Having made the replacement of $V_n^\alpha(q,k_H)$ by $V_n^\alpha(k_H)$, we may insert (2.3) into (2.2) and perform the q integration by evaluating residues, with the result that

$$e_\alpha^T = \frac{e^2}{\pi\hbar^3} \sum_{n=-\infty}^{+\infty} \int_{\bar{V}(k_H)>0} dk_H \, T_{\alpha\beta}(k_H,n)\, E_\beta\, e^{iq_n(k_H)L} \ , \tag{2.5a}$$

where

$$T_{\alpha\beta}(k_H, n) \equiv \hbar m^*(k_H)\, V_n^{\alpha}(k_H)\, V_n^{\beta}(k_H)^* / \bar{V}_H(k_H) \qquad (2.5b)$$

and

$$q_n(k_H) \equiv [\omega + n\omega_c(k_H) + i\gamma\,] / \bar{V}_H(k_H)\ . \qquad (2.5c)$$

In Eq. (2.5), the field is expressed in exactly that form implied by the discussion in Sec. I, namely, as an integral over all orbits for which electrons at the incident face of the slab move towards the emergent face. The field contributed by each orbit has its own spatial helix characterized by a q value, which is, aside from the damping term, exactly the same as that given in Sec. I. Also, the coefficient T (which we shall refer to as the "topological effectiveness" for reasons which will soon be apparent) describes the relative magnitude of the contribution to the transmitted field of electrons on the orbit at k_H. The only feature not stressed in Sec. I was the sum over n, which implies that electrons at a given k_H can also set up q values appropriate to the higher harmonics of the cyclotron frequency and that each of these has its own coefficient governing its strength. The form of this integral suffices to establish all the familiar properties of the GKO and the novel ones we observe as well.

B. GKO and Cyclotron Phase Resonance

Perhaps the most familiar form of GKO is that arising from a limiting point on the Fermi surface. The characteristic spatial dependence of that signal is $L^{-2}e^{iq(k_0)L}$, where k_0 is the value of k_H at the limiting point and $q(k_L)$ is the q value given by (2.5c) for $n = \pm 1$ and $\omega = 0$, the situation which Gantmakher and Kaner first studied.[8]

At a limiting point, the transverse velocity vanishes and the topological effectiveness is zero. To recover the Gantmakher-Kaner-type signal from the expression (2.5a), it is necessary only to expand both T and q to first order about their values at k_0,

$$q(k_H) = q(k_0) + (k_H - k_0)\, q'\ ,$$

$$T(k_H) = (k_H - k_0)\, T'\ ,$$

and to integrate over all k_H up to the limiting value $k_H = k_0$:

$$e^T \approx (T'/q'^2) L^{-2} e^{iq(k_0)L}\ .$$

This is not a particularly strong signal because it arises from a region of low topological effectiveness. Of more interest to us here is a signal which Gantmakher and Kaner attribute to the extremal helical trajectory. We can see how this signal arises, and at the same time demonstrate the phenomenon of cyclotron phase resonance by performing again an approximate evaluation of the integral in (2.5a).

As k_H sweeps through its allowed range, the phase

$$\Phi_n(k_H) \equiv L\ \mathrm{Re} q_n(k_H) \qquad (2.6)$$

sweeps through some range and the contribution of the various helixes tends to cancel. There may be a value of k_H for which Φ_n is stationary, however. In the neighborhood of such a value, many helixes from adjacent values of k_H all contribute in phase with each other, and a net nonzero field will result. The strength of the signal depends on how rapidly the various helixes get out of phase as k_H departs from the value at which the extremal value of Φ_n occurs. Equation (2.5) predicts a transmission peak which arises because the dephasing of the various helixes is slowest at cyclotron resonance. Let us examine this point in more detail. Suppose that there is a region of k_H over which m^* is nearly constant. We neglect the damping term $\gamma/\bar{V}_H$ for simplicity, and let k_n denote the value of k_H at which $q_n(k_H)$ has its extremum. That is,

$$\frac{d}{dk_H}\left(\frac{\omega + n\omega_c(k_H)}{\bar{V}_H(k_H)}\right)_{k_H = k_n} = 0\ . \qquad (2.7)$$

Then, an expansion of $q_n(k_H)$ in the neighborhood of k_n yields

$$q_n(k_H) = q_n(k_n) + \tfrac{1}{2} b_n (k_H - k_n)^2\ , \qquad (2.8a)$$

where

$$b_n = \frac{d^2}{dk_H^2}\left(\frac{\omega + n\omega_c(k_H)}{\bar{V}_H(k_H)}\right)_{k_H = k_n}\ . \qquad (2.8b)$$

At large L, the variation of phase with k_H dominates the integral (2.5a) which we can evaluate approximately as

$$e_\alpha^T \approx \frac{e^3}{\pi\hbar^3} \sum_n T_{\alpha\beta}(k_n, n)\, E_\beta e^{iq_n(k_n)L} \int dK e^{ib_n L K^2/2}$$

$$= \frac{e^2\sqrt{i}}{n\hbar^2} \sum_n \left(\frac{2\pi}{b_n L}\right)^{1/2} T_{\alpha\beta}(k_n, n)\, E_\beta e^{iq_n(k_n)L}\ . \qquad (2.9)$$

The factor $(2\pi/b_n L)^{1/2}$ appearing in (2.9) is exactly the range of k_H for which the phase is within $\pm\frac{1}{2}\pi$ of its extremal value. Clearly, this factor is the measure of how rapidly the various helixes lose phase coherence near $k_H = k_n$.

Consider the sequence of magnetic fields at which the various b_n vanish, namely, those fields for which

$$\omega_c(k_H) = -\omega/n\ . \qquad (2.10)$$

This series of field values, which will produce peaks in the transmitted intensities, is the same as that for which Azbel-Kaner cyclotron resonance occurs. However, the Azbel-Kaner resonance is a time resonance, in which electrons return to the field just at the right time to interact. The phenomenon here, on the other hand, is a phase resonance in which a large group of electrons with a wide range of $\bar{V}_H$ will arrive at the emergent face in phase with each other. We refer to this phenomenon as cyclotron phase resonance.

The amplitude of the transmitted signal at a given

cyclotron-phase-resonance field is proportional to the $T_{\alpha\beta}^{(n)}$ coefficient for that particular n. It can be shown, using (2.5b) and the definition of the V_n^α, that for orbits of fourfold rotational symmetry,

$$\sum_\beta T_{\alpha\beta}(k_H, n) E_\beta = 0 \quad \text{unless } n = 4j \pm 1 , \qquad (2.11)$$

where j is any integer or zero and the + or − sign is taken according to which sense of circular polarization is present in the incident fields (i.e., $E_x = \pm iE_y$). For linear polarization, Eq. (2.11) predicts that no cyclotron phase resonance will appear at even subharmonics of the fundamental resonance.

C. Signals Arising from Cutoff of Topological Effectiveness

In addition to the signals studied by Gantmakher and Kaner which are associated with either a limiting point or with a phase extremum, there is also the possibility of a signal arising from a rapid k_H dependence of the quantity $T_{\alpha\beta}(k_H, n)$. It is evident from the way that this quantity appears in Eq. (2.5a) that it is the measure of how effectively electrons at slice k_H on the Fermi surface extract energy from the driving-field component E_α and deliver it to the other side of the slab as a component to the transmitted current j_β. The definition (2.5b) contains factors which are consistent with this interpretation, namely, $V^\alpha(k_H)$, $V^\beta(k_H)$, and $1/\overline{V}_H(k_H)$, this last being proportional to the time the electrons spend in the skin depth and hence to the impulse they receive from the transverse field.

The $T_{\alpha\beta}^{(n)}$ depend on the details of the Fermi surface and on the direction of the magnetic field relative to the crystal axes, for the latter determines the orientation of the planes whose intersection with the Fermi surface defines the electron orbit in k space. The definition of the V_n^α is such that they are calculated by following the electron around its orbit, weighting each segment of the orbit by the time the electron actually spends in that section.[17] This feature also is consistent with the interpretation of $T_{\alpha\beta}$ as the measure of how effectively electrons extract energy from the field to deliver as a current. Because the $T_{\alpha\beta}$ are sensitive to the exact topology of the Fermi surface in the manner we have described, it will be convenient to refer to these quantities as "topological effectiveness" (T.E.).

The Fermi surfaces of the noble metals have sufficient structure as to make the $T_{\alpha\beta}$ strong functions of k_H. Here, we shall consider the situation in which the magnetic field is along a ⟨100⟩ axis of the crystal. In Fig. 2, we have sketched a typical noble-metal Fermi surface indicating the direction of the fields. The relevant topological features here are the eight necks which extend in the ⟨111⟩ directions. We speak of orbits whose plane k_H lies between the necks as "belly orbits," orbits whose plane lies beyond the necks as "polar orbits," and

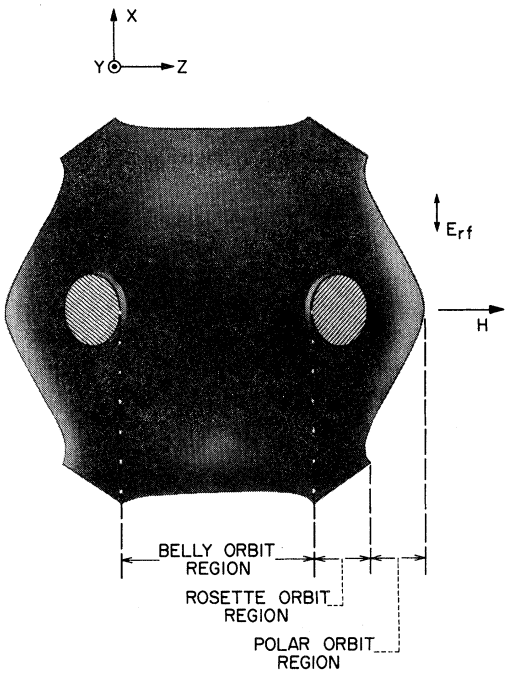

FIG. 2. Typical Fermi surface for a noble metal with H along a ⟨100⟩ direction, indicating three regions of different orbit types.

orbits whose plane is in the neck region as "rosette orbits." The rosette orbits, unlike the other two orbit types, are continuous only in the extended-zone scheme.

We have also indicated in Fig. 3 a typical T.E. for k_H in the polar-orbit region. The functional dependence of the T.E. on k_H is easily understood. At the pole of the Fermi surface (a ⟨100⟩ direction in this case), the Fermi surface is normal to H and the electron velocity is along H. Since there is no transverse velocity, the electron can extract no energy from the transverse rf field and the T.E is zero. As k_H is reduced, electrons acquire transverse velocity and their T.E. rises until k_H approaches the boundary between the rosette-orbit region and the polar region.

Electrons on a polar orbit passing close to the necks, such as the one beneath the arrow, traverse that orbit in $\vec{k}$ space at a varying rate ($\dot{\vec{k}} = q\vec{V} \times \vec{B}/\hbar$). As an electron approaches one of the ⟨111⟩ necks, its velocity $\vec{V} = \nabla_k \epsilon$ tips toward the z direction, reducing its transverse velocity, thereby lowering its effectiveness. In addition, the lowering of its transverse velocity lowers its $\dot{k}$, so that it spends more than an average amount of time in this region. This effect *markedly* decreases the effectiveness, since the electron spends most of its time in the state where it is least able to gain energy from the field. Hence, the effectiveness of polar orbits drops as their k_H approaches the

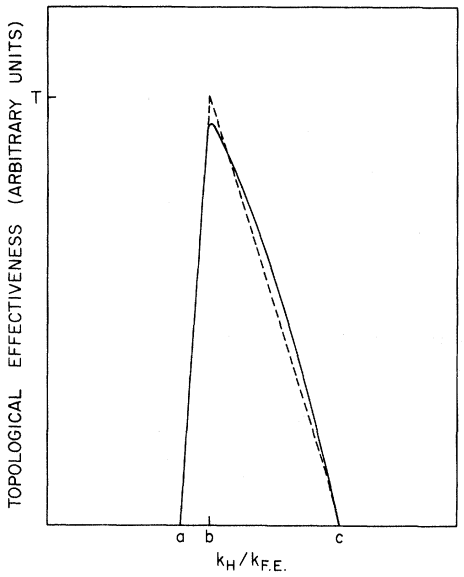

FIG. 3. Typical graph of the topological effectiveness as a function of k_H, for the polar electrons of a noble metal with H along ⟨100⟩. The dashed lines represent an approximation described in the text.

onset of the rosette region.

We can now see how the T.E. mechanism gives rise to a GKO. For the case of a sharply peaked T.E. curve, as is the case for the polar electrons of copper and silver, the wave vector of the GKO is that appropriate to a slice of Fermi surface whose k_H value is given by the peak of the T.E. curve. This may be most simply demonstrated by the following idealized case of a T.E. curve of triangular shape (Fig. 3), that is,

$$T_{\alpha\beta} = \begin{cases} 0\,, & k_H < a & \text{(2.12a)} \\ T(k_H - a)/(b-a), & a < k_H < b & \text{(2.12b)} \\ T[1-(k_H-b)/(c-b)], & b < k_H < c & \text{(2.12c)} \\ 0\,, & c < k_H\,. & \text{(2.12d)} \end{cases}$$

Here a is the value of k_H at the boundary between the rosette orbits and the polar orbits, b is the value of k_H at the plane of maximum effectiveness, c is the value of k_H at the pole, and T is the value of the T.E. at its maximum. We expand $q_n(k_H)$ to first order about $k_H = b$:

$$q_n(k_H) = q_n(b) + (k_H - b)\,q'\,. \tag{2.13}$$

Using (2.12) and (2.13), we evaluate

$$\int T(k_H)\, e^{iq_n(k_H)L}\, dk_H$$

$$= \frac{Te^{iq_n(b)L}}{iq'L}\left(\frac{e^{-q'L(b-a)}-1}{(b-a)iq'L} + \frac{e^{iq'L(c-b)}-1}{(c-b)iq'L}\right). \tag{2.14}$$

We are interested in the situation where the T.E. falls so rapidly in the region of k_H between the maximum and the cutoff that the phase of the emergent current changes only slightly with k_H, while at the same time, the rather broad region over which the T.E. effectiveness builds as k_H moves in from the pole is wide enough for the phase of the emergent current to change appreciably. In this case, the denominator of the first term in (2.14) will be small, that of the second will be large, and we will have

$$\int T(k_H)\, e^{iq_n(k_H)L}\, dk_H = iTe^{iq_n(b)L}/(q'L)\,. \tag{2.15}$$

That is, we have a signal caused by the sharpness of the T.E. cutoff, characterized by the effectiveness and the phase of those electrons located at the slice of maximum effectiveness.

III. ORBITAL PARAMETERS

In this section, we shall present graphs of some of the orbital parameters which are central to the discussion of Sec. II and which will be needed in order to support some of the conclusions drawn in Sec. V. The quantities here are combinations of those which appear in the conductivity tensor (2.3) derived by Overhauser and Rodriguez.[17] Our notation differs somewhat from that of Overhauser and Rodriguez, but the correspondence

$$\begin{aligned} &eH/m^*(k_H)\,c = \omega_c(k_H) \to 2\pi/T(E,k_z)\,, \\ &V_n^{\alpha}(q,k_H) \to V_n^{\alpha}(E,k_z)\,, \\ &\overline{V}_H(k_H) \to V_s(E,k_z) \end{aligned} \tag{3.1}$$

establishes the definitions of the quantities we use here. Our computation is exactly that which is implied by the definitions given in Ref. 17 for the quantities on the right-hand side of the arrows in (3.1).

The basic input to the programs was Halse's model for the Fermi surface of the noble metals.[11] We utilize Halse's Fermi radii and Fermi speeds at the various angles (with respect to the center of the Brillouin zone) for which he has provided values, and we used a quadratic-interpolation scheme to evaluate those derivatives which are needed to specify the direction normals to the Fermi surfaces, so that we can determine velocities at each point on the Fermi surface. Orbits (k_x and k_y pairs which lie on the Fermi surface when k_z is specified) were determined by quadratic-interpolation formulas. All calculations are carried out for H along a ⟨100⟩ direction.

In Figs. 4 and 5, we present graphs of $m^*(k_H)$, $\overline{V}_H(k_H)$, and $2\pi m^*(k_H)\,\overline{V}_H(k_H)/\hbar$, this last quantity being calculated here as the indicated product. It is known, however, that

$$-2\pi m^*(k_H)\,\overline{V}_H(k_H) = \hbar\left(\frac{\partial A}{\partial k_H}\right)_E,$$

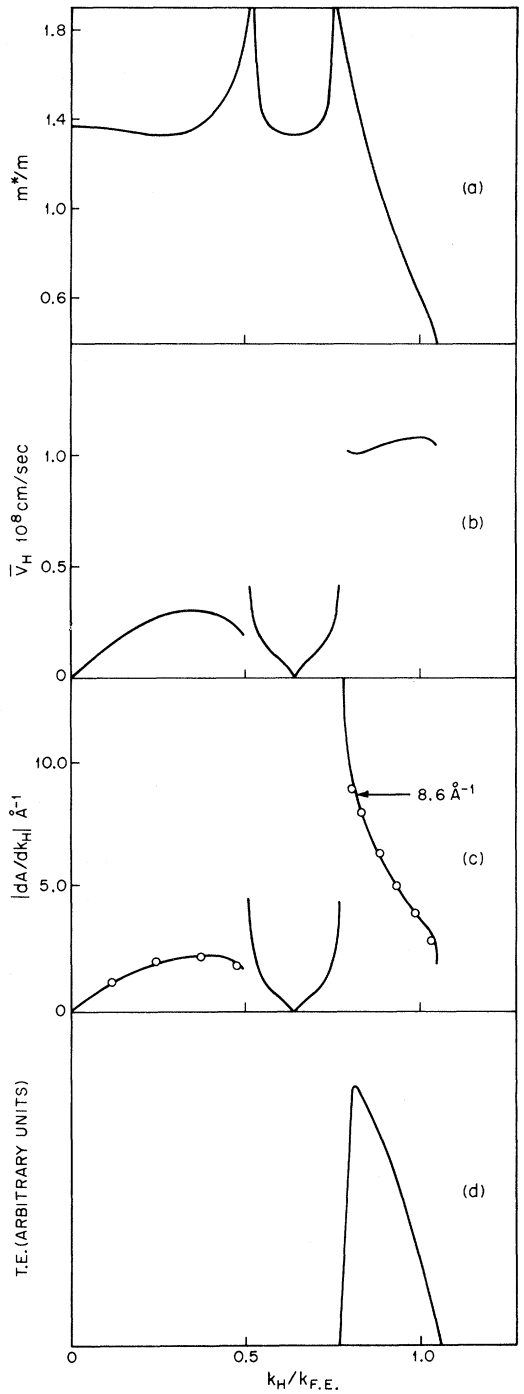

FIG. 4. Fermi-surface parameters for {100} copper; (a) the effective mass, (b) the velocity along the field, (c) the parameter $|dA/dk_H|$, (d) the topological effectiveness, in arbitrary units, and for the polar electrons only.

where A is the cross-sectional area of the Fermi surface. Thus, this last quantity could have been calculated directly from the Fermi-surface data without making use of Fermi speeds, direction normals, or integration of the equations of motion, all of which were required to compute m^* and $\bar{V}_H$ separately. We have indicated values of $\partial A/\partial k_H$ calculated directly as points on the same curve, which provides a partial check of at least some aspects of our calculation. The quantity m^* is given in units of the free-electron mass; k_H is given in terms of the free-electron Fermi wave vector k_{FE}.

In Figs. 4(d) and 5(d), we are concerned with the T.E. defined by Eq. (2.5b), evaluated for polar orbits. It is especially useful to calculate the T.E. for the circularly polarized components, namely,

$$T_{xx}^{\pm n} + iT_{xy}^{\pm n} \equiv T_{\pm n} .$$

In Figs. 4(d) and 5(d), we have plotted T_1 for copper and for silver. The important quantity here is the location of the peak. The units in which T is expressed are arbitrary.

IV. EXPERIMENTAL TECHNIQUES

The technique of microwave-transmission spectroscopy has been described by both Lewis and Carver[18] and Shultz and Dunifer.[19] Both of these groups of authors have employed spectrometers operating in the 10-GHz frequency band. We discuss here a spectrometer operating at 35 GHz, describing briefly those aspects that are similar to the spectrometers of Refs. 18 and 19, and in slightly greater detail those aspects that represent innovations.

The previous authors have used a superheterodyne detection scheme in conjunction with room-temperature diode crystal detectors, whereas we use a homodyne scheme with a liquid-helium-cooled Kinch-Rollin[20] InSb hot-electron bolometer which we operate as a detector in a mixing mode. This detection scheme has been operated by us up to frequencies of 120 GHz with minimum detectable signal powers of 10^{-21} W in a one-cycle bandwidth. Thus we have a power detectivity superior to that obtainable at 10 GHz by conventional techniques (10^{-19}–10^{-20} W), which can be maintained up to the highest frequencies to which we have so far applied the techniques of transmission spectroscopy. Reports of work carried out at 120 GHz and details of the detection scheme for a bolometer mixer will be presented elsewhere.

A block diagram of the 35-GHz spectrometer is shown in Fig. 6. A 500-mW klystron provides the signal power, amplitude modulated at a frequency of 10 kHz by a ferrite modulator, and also the reference power which is not modulated. The signal power is fed into a cryostat where it is coupled into the upper or driving TE_{110} (rectangular) cavity whose end wall is formed by one surface of the metal crystal specimen to be investigated [see Fig. (6)]. A second similar (receiving) cavity is positioned below the first, such that the microwave

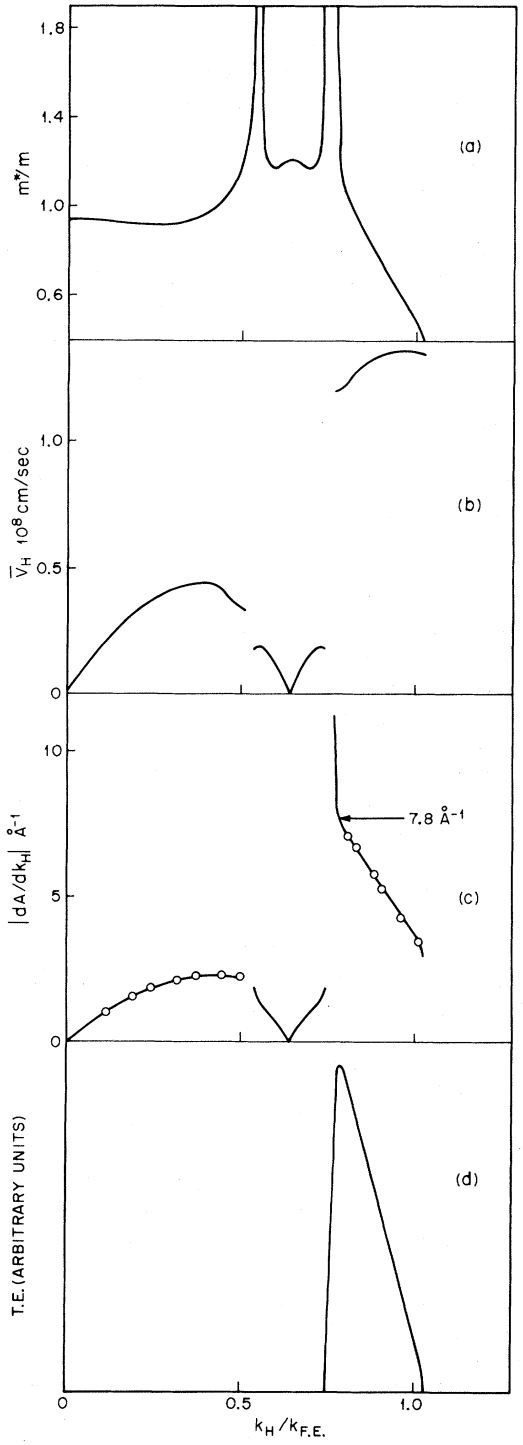

FIG. 5. Fermi-surface parameters for {100} silver.

magnetic field at the surface of the transmission specimen is parallel to the equivalent field in the driving cavity. These two cavities are brought to the same frequency by means of a tuning slug in the top cavity. The receiving or lower cavity is coupled to a waveguide-mounted-InSb bolometer detector at the bottom of the cryostat and the bolometer is backed by an adjustable waveguide reflector. A directional coupler also feeds the reference power to the detector through this waveguide. The bolometer and auxiliary circuitry are surrounded by a superconducting screen to prevent any field dependence of the detection scheme.

The entire system of cavities, bolometer detector, and associated circuitry is enclosed in a vacuum space which can be filled with helium exchange gas. Most measurements have been taken at 4.2 K, although facilities exist which enable us to cover the temperature range 1.3–50 K. In the geometry of the experiments described here, a magnetic field is provided normal to the plane of the specimen by means of an axial superconducting solenoid. This field is also normal to the microwave magnetic fields at the two surfaces of the specimen.

For this experiment we choose our TE_{110} rectangular-cavity mode such that it is nondegenerate with any other mode, and the detection scheme is therefore only sensitive to radiation of a particular linear-polarization direction. Also, since our detector operates in the mixing mode, we are sensitive to that component of the electromagnetic field, transmitted through the specimen, which is in phase with the reference field. The phase angle between the reference field and the driving field is an important quantity in the experimental measurements, and it is a function both of the properties of the specimen and of the spectrometer. The part due to the spectrometer can be varied by means of a microwave phase shifter in the reference arm. Thus the 10-kHz signal from the bolometer con-

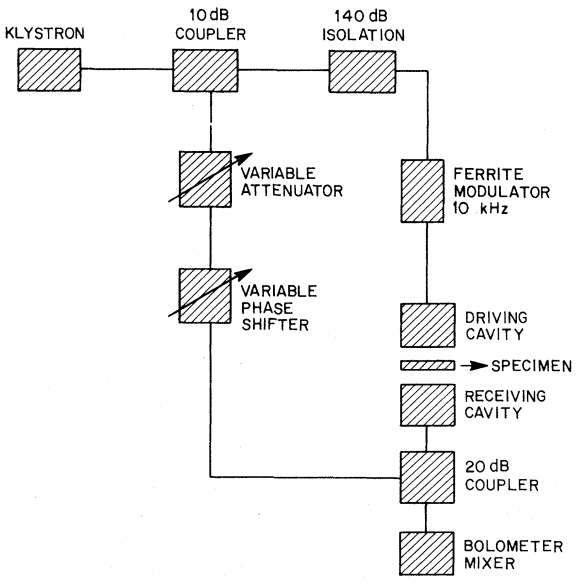

FIG. 6. Block representation of the 35-GHz spectrometer.

tains both phase and amplitude information. This signal is amplified and detected by a lock-in detector whose reference input is driven from the same oscillator that drives the microwave modulator. The output of the lock-in detector is plotted on the y axis of a recorder whose x axis represents the dc magnetic field on the specimen.

The sensitivity to transmitted signals, in this experiment, is ultimately limited by the detector noise (10^{-21} W/Hz). However, this condition is not normally achieved, since the presence of modulated radiation leaking around the sample into the receiving cavity introduces klystron noise and spectrometer thermal drifts. This is eliminated as far as possible by using indium gaskets between the sample and the cavities. With a klystron input power to the driving cavity of 10^{-1} W it was found possible to reduce the leakage power to about 10^{-19} W.

The specimens used in this experiment were single-crystal slices of both copper and silver, and were cut from ingots whose resistivity ratios ($R_{290\,K}/R_{4.2K}$) were approximately 20 000 for the copper ingot and 5000 for silver. The particular technique used to slice the crystal ingots was found not to be important, provided the strain and damage layers at both surfaces were removed. Various methods were used to remove the strain layer including chemical etching, electrolytic polishing, and ion milling. Of these the most satisfactory proved to be low-energy ion milling (ion energies <10 keV) in that a strain free flat surface can be obtained on samples whose thickness may be as little as 10 μ. Ion milling is a technique more commonly used for preparation of samples for electron-diffraction microscopy, and consists of an ion beam (generated by a plasma gun), which is allowed to impinge on the specimen at an oblique angle thus gradually removing material. We achieve sample flatness by continuous motion of the sample in two dimensions. This motion averages out the intensity variations across the ion beam.

For this experiment the sample thickness varied between 1 mm and 50 μ and measurements were made with a bench micrometer whose accuracy was better than 1 μ. All samples were oriented with the plate normal along or near a crystallographic $\langle 100\rangle$ axis, and were checked by x-ray reflection techniques.

V. RESULTS AND DISCUSSION

Transmission experiments of the type described in Sec. IV have been carried out by us for many metals of high purity. The results we present here are for copper and silver only, and indeed for just a $\langle 100\rangle$ crystallographic axis parallel to the field. We feel that these results exhibit several of the many possible manifestations of microwave transmission as discussed in this paper and may be considered representative of transmission in the field normal geometry. We observe the conduction-electron spin-resonance signal in both copper and silver, but do not comment here since the subject has been treated by Shultz and Latham.[21]

The first observation, which seems to be typical of many metals, is of a transmitted field which is oscillatory as a function of dc field as in Fig. 7. This transmitted signal has a dependence on the microwave phase of the reference signal which is characteristic of these microwave GKO, but is not as simple as our theoretical discussion would suggest. Experimentally the major portion of the spectrum, from usually one or two kilogauss to the highest fields shown, shifts in phase in exact correspondence with the phase of microwave phase shifter in the reference arm. However, the very-low-field signals do not change phase, but rather show an amplitude variation as a function of the reference phase.[22] This behavior is sometimes partially obscured by the presence of more than one type of oscillation. The theory of Sec. II gives the transmitted field as of the form

$$F_\alpha = \sum_{n=-\infty}^{\infty} A_\alpha^{(n)}\, e^{-L/\lambda}\, e^{i[(\omega+n\omega_c)L/\bar{V}_H+\varphi_n]}, \qquad (5.1)$$

where ω_c and $\bar{V}_H$ appearing here are those appropriate to the dominating slice of Fermi surface, i.e., the slice for which the phase is extremal or the T.E. is maximal.

For convenience of discussion we have written the amplitude in (5.1) as the product of a real magnitude $A_\alpha^{(n)}$ and a phase $e^{i\varphi_n}$. Several physical phenomena contribute to φ_n. First, the dynamics of the self-consistent screening of the incident fields may result in a launching field whose direction dif-

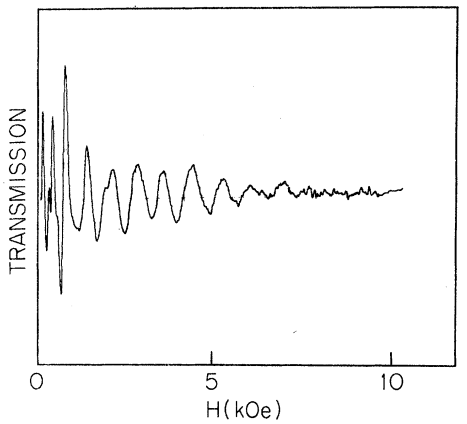

FIG. 7. Transmitted signal amplitude as a function of dc magnetic field. The field is normal to a sheet of copper, 0.905 mm thick, which is oriented such that its normal is along a $\langle 100\rangle$ axis. Signal amplitude is in arbitrary units.

fers from that of the incident field. Therefore the impulse given to the ineffective electrons responsible for transmission may not lie in the direction of the driving field. This is equivalent to a phase shift. A similar effect takes place at the receiving surface. According to our assumption (v) of Sec. II this effect is not a function of magnetic field, but this assumption may break down for cyclotron resonance in the screening currents. Another contribution to φ_n arises from the manner in which various helixes add to give a resultant field, e.g., whether the extremal phase leads or lags its neighbors. This effect may be field dependent at cyclotron phase resonance. Consequently, for a given GKO, we may consider the φ_n as field independent away from any regions of resonances in the transmission.

To interpret the experimental transmission we note that the receiving cavity responds only to linear (say the x direction) polarization, and that the signal is mixed with a large reference signal, derived from the driving field, but shifted in phase by an amount φ_0. This phase shift may be varied by means of the phase shifter in the bias arm. Thus we detect a signal

$$S \propto \sum_{n=-\infty}^{\infty} A_x^{(n)} e^{-L/\lambda} \cos[(\omega + n\omega_c)L/\overline{V}_H + \varphi_n - \varphi_0]. \quad (5.2)$$

In the case of a sinusoidal signal we have only the values $n = \pm 1$ to consider, and if the Gantmakher-Kaner field contains only one sense of circular polarization (say left handed) then only $n = -1$ appears in (5.2). The signal is then of the form

$$S \propto A_x^{(-1)} e^{-L/\lambda} \cos[(\omega - \omega_c)L/\overline{V}_H + \varphi_{-1} - \varphi_0]. \quad (5.3)$$

It is clear from this expression that the phase of the GKO signal depends linearly on φ_0 when there is only one sense of circular polarization present. This corresponds with the observed behavior at high magnetic fields. We therefore deduce that in this region of the spectrum the transmission is dominated by one sense of circular polarization.

In the case of linearly polarized transmission, components $n = \pm 1$ are both present, and since at zero or low magnetic field the transmission cannot distinguish between these two senses they must be present with equal amplitude, i.e., $A_\alpha^{(1)} = A_\alpha^{(-1)}$. The expression equivalent to (5.3) is then

$$S \propto A_x^{(1)} e^{-L/\lambda} \cos[\omega L/\overline{V}_H + \tfrac{1}{2}(\varphi_1 + \varphi_{-1}) - \varphi_0] \times \cos(\omega_c L/\overline{V}_H). \quad (5.4)$$

This GKO is a signal whose phase is independent of φ_0, but whose amplitude is an oscillatory function of the spectrometer microwave phase shift. This corresponds to the low-field behavior in the experiment.

We conclude then that the observed behavior is due to the absence of one sense of circular polarization at high magnetic fields. The theory of Sec. II provides no mechanism for this effect, except that the cyclotron phase resonance favors only one sense of circular polarization. However, the effect appears to be more general since it is not constrained to field regions near a resonance. The wings of a phase resonance, while providing a weak mechanism, do not appear to be able to account for the effect. The origin may well be concerned with the details of the driving process in an anisotropic Fermi-surface material, which falls outside the scope of this article for reasons stated in Sec. II.

A. Thick Specimens of Copper and Silver

Figures 7 and 8 show transmission spectra for {100} specimens of copper and silver which are approximately 1 and $\frac{1}{4}$ mm, respectively, in thickness. We describe these specimens as thick in that the signal is weak and rapidly decreases for thicker specimens, indicating that the specimen thickness is comparable with or greater than the longest electronic mean free path across the sample.

We may gain insight into the likely origin of the signal in this regime of thickness by examining the velocity along the field for a {100} specimen. From Figs. 4(b) and 5(b) we see that the fastest electrons are those in the polar region and that the velocity of these electrons is reasonably constant throughout this region. Figures 4(c) and 5(c) show that there is no extremal of dA/dk_H in this region so that it is not likely that the oscillation is of the simple extremal-helical-trajectory GKO variety. It might be thought that the oscillation is due to the limiting-point (LP) electrons, but we may easily demonstrate that this is not the case, and that it is, in fact, an example of an oscillation produced by a peak in the T.E.

The field spacing for a phase change of 2π in

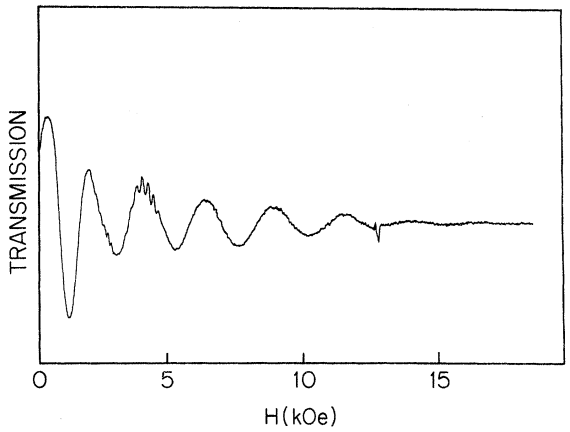

FIG. 8. Transmitted signal for a {100} sheet of silver 0.25 mm thick.

the oscillations is given by expression (5.2) as

$$\Delta H_n = \frac{2\pi |m^* \bar{V}_H|_E}{eL} \frac{c}{n}, \tag{5.5}$$

where the extremal value is determined by (2.7) for the extremal helical trajectory (EHT) case, and directly by the Fermi surface for the LP or T.E. cases. We may now define a quantity

$$k_n^* = \Delta H_n \frac{eL}{c\hbar} = \frac{2\pi}{n\hbar} |m^* \bar{V}_H|_E, \tag{5.6}$$

which characterizes those electrons on the Fermi surface responsible for the particular experimental signal. k_n^* may be a function of H, in the EHT case, but not for LP or T.E. cases.

From the experimental data we find that k_n^* is not a function of H and has a value of $8.6(\pm 0.1)$ Å^{-1} for copper and $7.8(\pm 0.2)$ Å^{-1} for silver, for the fundamental oscillation ($n=1$). From the Fermi-surface calculations of Sec. III we find that these values correspond to $k_H = 0.80 k_{FE}$ for copper and $0.78 k_{FE}$ for silver. These values agree well with the peaks of the T.E. curves of Figs. 4(d) and 5(d), and rule out the possibility that the LP electrons are involved. It is interesting to note that the recent results of Wood and Gavenda,[23] for {100} copper, show an effect in a D.S.C.R. helicon absorption edge which originates from a point on the Fermi surface close to $0.8 k_{FE}$. They give no explanation for this effect, but we feel it is likely to be due to the same variation of T.E. we see here.

B. Time-of-Flight Measurement of Fermi Velocity

We now return to the interesting question of the phase of the GKO and the observation that the time of flight for electrons crossing the sample is comparable with the microwave period. We have established experimentally that the microwave phase corresponds directly to the GKO phase, apart from an unknown constant term, at least when we confine our attention to the spectrum above 2 kG. From expression (5.3) we may write the phase as

$$\varphi = \frac{\omega L}{\bar{V}_H} + \varphi_{-1} - \varphi_0 - \frac{\omega_c L}{\bar{V}_H}.$$

The term in $\omega L/\bar{V}_H$ is due to the time delay of the unscattered-electron passage across the sample. The last term is linearly dependent on the field H and is, of course, responsible for the sinusoidal variation of the transmitted signal. If we can separate these various contributions and determine the time-of-flight term we would have a direct measure of $\bar{V}_H$, since ω and L are measured in the experiment.

We may eliminate the field-dependent term $(\omega_c L/\bar{V}_H)$ by extrapolating the GKO transmitted-signal phase to $H=0$. Extrapolation is necessary because the low-field region contains linearly polarized waves and does not appear as a simple sinusoidal signal. It is possible to make such an extrapolation only if there are no other field-dependent terms present. Also the phase shift φ_{-1} may be field dependent near a resonance. Oscillations which show such a resonance would be difficult to analyze from this point of view.

A knowledge of $\varphi_{H=0}$ is not sufficient to determine $\omega L/\bar{V}_H$ since φ_{-1} and φ_0 are unknown. However, measurements made for a set of samples of varying L will provide enough information to eliminate $\varphi_{-1} - \varphi_0$. The results for such a set of measurements are shown in Fig. 9. A considerable number of points were obtained to establish the techniques and to eliminate the uncertainty of 2π times an integer which is present in each point. In future measurements it would seem that velocities could be obtained with the use of only two specimens, provided they were sufficiently close in thickness to give a phase change of less than 2π. In fact the measurements of Fig. 9 were actually determined from one {100} copper sample which was gradually etched down through the range of thicknesses indicated. This technique helped to guarantee that the crystallographic axes of all specimens were identical.

The value obtained for $\bar{V}_H$ of 1.03×10^8 cm/sec is in good agreement with the value of 1.02×10^8 cm/sec obtained from the Fermi-surface data for an orbit with a k_H of $0.8 k_{FE}$. This helps to confirm the original identification of the GKO.

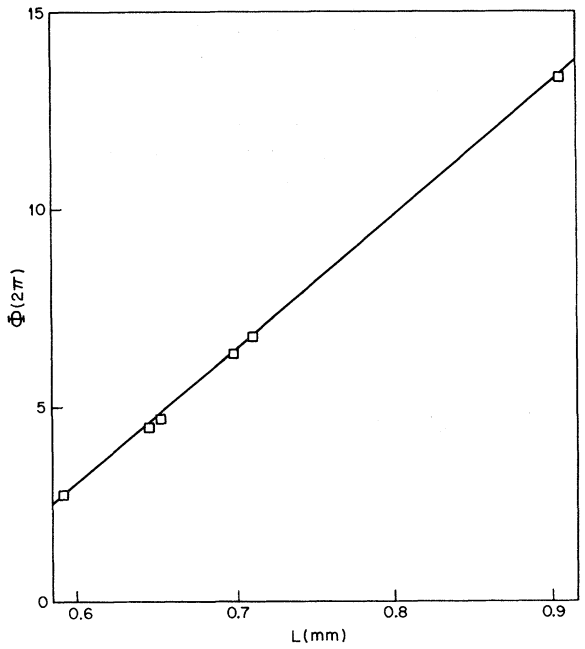

FIG. 9. Plot of the extrapolated microwave phase at zero magnetic field as a function of sample thickness.

C. Intermediate Thickness Samples

So far we have discussed samples for which the fastest electrons only have been able to cross the sample without scattering. Indeed, a mean-free-path mechanism could act, in certain circumstances, to provide a cutoff in the electron helix distribution and so give yet another form of GKO. We would not expect this behavior here since the velocity $\overline{V}_H$ of the polar electrons is essentially constant [see Figs. 4(b) and 5(b)] as a function of k_H, but we have selected against the considerably slower electrons on orbits not in the polar region.

As the samples are reduced in thickness the first noticeable effect is that the intensity of the GKO increases. Unfortunately we cannot make any quantitative measurements of this increase since the scattering time, as measured by the resistance ratio, does not remain quite constant from sample to sample. This is due to unavoidable differences in handling processes.

A second and more striking effect is the gradual increase in relative intensity of a new set of oscillations. Initially these appear as fine-structure oscillations at low fields, superimposed on the polar-electron GKO as shown in Fig. 10, and as the samples are made even thinner grow to dominate the spectrum. This occurs most clearly in the case of copper as in Fig. 11. A high-field oscillatory burst also becomes clearly observable at the thickness of Fig. 11, and the spectrum has taken on a totally new appearance.

From the thickness dependence of the spectrum we can deduce that these oscillations are due to electrons whose mean free path, and therefore presumably whose velocity across the sample, is considerably less than that of the polar electrons. The amplitude domination of these oscillations over those of the polar GKO requires explanation as does their unusual field dependence. These questions

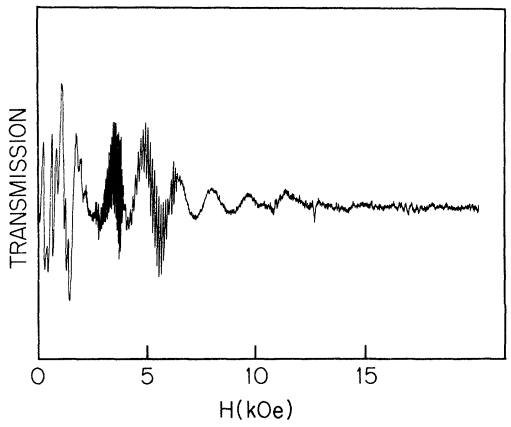

FIG. 10. Transmitted signal for a {100} copper sample of thickness 0.43 mm.

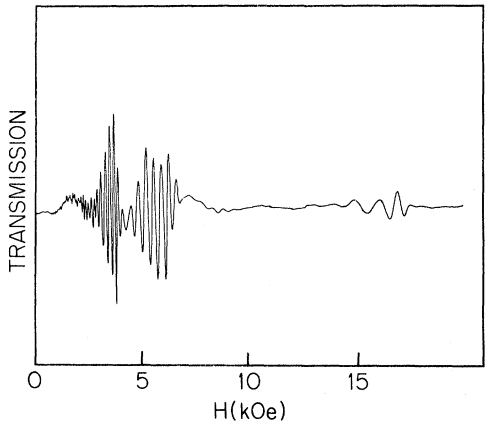

FIG. 11. Transmitted signal for a {100} copper sample of thickness 0.137 mm.

are answered by the experiments of Sec. V D.

D. Thin Samples and Transmission Resonances

The first thin sample ($L = 0.074$ mm) of {100} copper which was examined in transmission showed a most striking spectrum, Fig. 12(a). The oscillatory bursts had sharpened into apparently resonance features whose field values could be characterized, and it became clear that the oscillatory bursts at low fields were harmonics of the high-field resonance. Phase information is initially confusing here and the centers of the resonances are more easily found in a power spectrum [Fig. 12(b)] which was obtained by running the bolometer as a video detector, i.e., zero-microwave-bias power. The system is considerably less sensitive in this mode of operation (minimum detectable signal $\sim 10^{-13}$ W in a one-cycle bandwidth), but the resonance transmission (~ -100 dB) for this specimen was much greater than the GKO transmission strength of thicker samples (~ -160 dB for the sample of Fig. 7).

The centers of the resonances, as defined by the peaks in the power spectrum, fall at a set of magnetic field values given by

$$H_n = (m^*c/ne)\,\omega_0 , \qquad (5.7)$$

where $m^*/m = 1.34(\pm 0.01)$ and n takes the values 1, 2, 3, 4, 5, 7, and 9 for the clearly defined resonances. Weaker resonances are more easily observed in the mixer-detection-scheme results of Fig. 12(a).

It is surprising to find even values for n in this series since, from (2.11), harmonic generation should be confined to those values of n given by

$$n = j\,\alpha \pm 1 ,$$

where j is an integer and $\alpha = 4$ for the fourfold symmetry of a ⟨100⟩ axis. It was later found that the

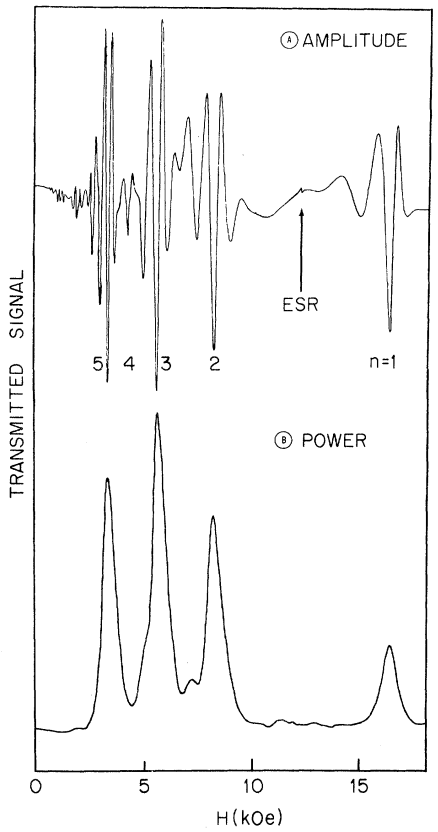

FIG. 12. (a) Transmitted signal amplitude for a copper sample of thickness 0.074 mm. (b) Transmitted signal power. For this sample the normal to the plate was approximately 2° from a ⟨100⟩ axis.

even values were due to a 2° misorientation of the crystal and were not present in specimens oriented to better than $\frac{1}{2}°$.

Similar resonances were observed for silver crystals, but with somewhat lower intensity. A specimen of thickness $L = 0.095$ mm shows a spectrum (Fig. 13) which is similar to the intermediate-thickness specimens of copper, the polar-electron GKO being clearly observable. In this case the specimen is accurately oriented along a ⟨100⟩ axis and only odd harmonics are observed. The mass value for these resonances, as defined by expression (5.7), is $m^*/m = 0.92(\pm 0.02)$.

These resonant bursts of transmitted field have some connection with cyclotron resonance as is clear from Fig. 12, but are not to be confused with Azbel-Kaner cyclotron resonance which takes place in a totally different geometry. In fact they are examples of what we have called a phase resonance, where the wavelength of the electron helix becomes infinite and all the propagating-electron phases add constructively.

In the simple case discussed in Sec. II, a region of constant mass on the Fermi surface will give rise to a resonant transmission at values of the magnetic field given by

$$\omega_0 = n\omega_c ,$$

where n takes the values $4j \pm 1$ for a ⟨100⟩ axis, and j is an integer. The relative intensity of the resonances n should then depend on the size of the coefficients V_n in the Fourier transformation of the orbits. In the case of copper, we know from cyclotron-resonance and de Haas–van Alphen data that the electron mass is only slowly changing as a function of orbit position on the Fermi surface, when close to the belly. Also the belly mass[11, 24] is close to the value we observe here of 1.34 m. We also know[11] that the orbits near the belly are well represented by j values of 0 and 1, so that we might expect strong resonances $n = 1, 3$, and 5 in agreement with experiment. However, Fig. 4(a) shows that there is a region of flat mass in the rosette-orbit section of the Fermi surface, which is nearly degenerate with that of the belly electrons. The low velocity of these holes [Fig. 4(b)] would lead us to suspect that they are not responsible for the effect, and, as we shall see later in this section, the phase dependence is closely what we should expect for belly electrons. Any ambiguity remaining is removed by examination of the case of silver. Here the experimental-mass value of 0.92 m is very close to the mass of the belly electron [Fig. 5(a)], whereas the rosette-orbit masses are quite different.

Since the resonances appear to be associated with the nearly-constant-mass region of the belly orbits, we examine that region of the Fermi surface with care (Fig. 4), and notice that there is a maximum in dA/dk_H or $m^* \bar{V}_H$ in the vicinity. That is to say, there would be present, at low frequencies, a GKO of the EHT variety with an appropriate value of wave vector for that value of k_H (see Perrin,

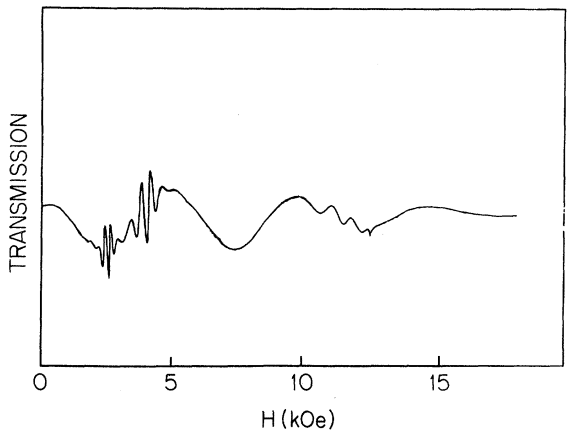

FIG. 13. Transmitted signal amplitude for a {100} silver sample of thickness 0.095 mm.

Weisbuch, and Libchaber[25]). At high frequencies the k_H value for the GKO is determined by (2.7). In a region of constant mass ($\partial\omega_c/\omega k_H = 0$) this result reduces to

$$(\omega \pm n\omega_c)\ \frac{\partial(1/\overline{V}_H)}{\partial k_H} = 0\ ,$$

which, for arbitrary magnetic field, is the same as the low-frequency result. Even in the vicinity of phase resonance the simple analysis embodied in Eq. (2.9) predicts that the portion of Fermi surface contributing to transmission is still determined by the EHT condition, and so we might expect the oscillation period within the bursts; i.e.,

$$k_n^* = (2\pi/n\hbar)\,|m^*\,\overline{V}_H|_{\mathrm{EHT}}\ ,$$

to have the value found in the low-frequency experiments. However, this is only approximately the case for copper. No low-frequency data is available for silver.

In order to analyze the difficulties in the simple theory, we should consider again the general condition (2.7) for the EHT GKO. The solution to this equation can be regarded as specifying which orbits k_H on the Fermi surface give rise to the signal for a given value of H. Such solutions for copper and silver indicate that large regions of Fermi surface in the belly region contribute to the signals at phase resonance. This is in agreement with the observation that resonances are associated with regions of flat mass on the Fermi surface. This also means, unfortunately, that a full integration over the relevant region of Fermi surface must be carried out [Eq. (2.5)] in order to find the transmitted field as a function of magnetic field, i.e., that the simple description embodied in Eq. (2.9) is inadequate. Such calculations have been carried out for copper, and the results are shown in Figs. 14(a) and 14(b). The calculations are made for thicknesses appropriate to the experimental specimens of Figs. 11 and 12, and we have assumed a scattering time of 10^{-9} sec. We made comparison only with the fundamental resonance ($n = 1$).

It appears that there is only qualitative agreement between the calculation and experiment. The calculated transmission peaks at a mass value of about 1.37 m, whereas the experimental value is 1.34(±0.01) m. Also, the theoretical transmission is not quite as sharply peaked as the experimental resonance, having a low-field tail which is more extensive. However, the phase dependence agrees reasonably with the value of $nk_n^* = 2.1$ Å^{-1} for copper (the corresponding value for silver is 2.0 Å^{-1}). The low-frequency GKO value of Perrin, Weisbuch, and Libchaber[25] is 2.3 Å^{-1}. In the case of silver the calculated spectrum peaks at a mass of 0.93 m, to be compared with the experimental value of 0.92 m. However, the experimental signals are not sufficiently well defined to make useful a more detailed comparison.

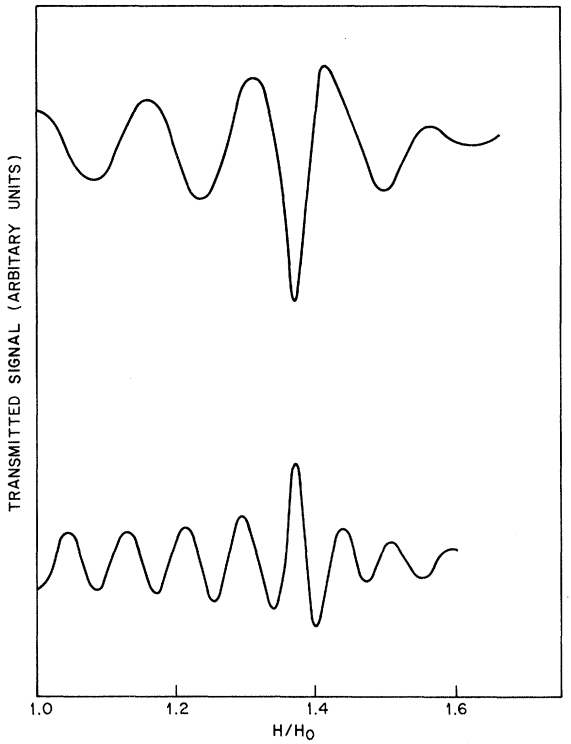

FIG. 14. Calculated transmission amplitudes, in arbitrary units, for the fundamental resonances ($n = 1$) of the specimens of Figs. 11 and 12. H_0 is the field for free-electron cyclotron resonance.

There are probably several factors which prevent exact agreement between experiment and calculation for these resonances. The intensity and line shape may be controlled to some extent by the driving process. That is, the behavior of the currents in the skin depth under conditions of resonance may act to partially screen the electromagnetic fields from the sample. Effects of this type have been totally omitted in the simple theory presented here. There is also an experimental effect which is hard to eliminate and which is due to the lack of flatness and parallelism in the samples. This results in a tendency for high-q oscillations ($qL > \frac{1}{2}\pi$) to give reduced signals at the second surface due to variations in phase across the sample. The effect is not present at the center of the resonance ($q \approx 0$), but gets progressively stronger as one goes further into the wings of the resonance. Thickness variations of the order of 5 μ are present in the samples of Figs. 11 and 12, and would lead to sufficient line narrowing to explain most of the line-shape difference between experiment and theory. It is an experimental fact that specimens with gross thickness variation show sharp and intense phase resonances but very reduced GKO intensity.

VI. CONCLUSIONS

The microwave transmission through {100} sheets of copper and silver, as a function of dc magnetic field normal to the sheet, has been shown to consist of two basic types of signals. For samples which are sufficiently thick that only the fastest electron can cross the sample without scattering a Gantmakher-Kaner oscillation results. For thin samples, where a significant fraction of the electrons on the Fermi surface can reach the second surface without scattering, a harmonic series of resonant-transmission bursts occurs. It has been shown that both of these signals are due to single-particle propagation and a simple theory has been given which allows a unified description of these effects.

It has been shown that the use of microwave frequencies allows one to determine Fermi velocities by a time-of-flight technique and this was demonstrated for the electrons responsible for the GKO in thick copper samples. The velocity determined in this way was in agreement with the value given by Halse. In fact the GKO signals in thick copper and silver are due to electrons on orbits which are neither of an EHT type, nor of a LP type, and it was shown that these orbits correspond to a peak in the T.E. as a function of k_H. Agreement between experiment and theory is satisfactory for the thick samples except for the polarization of the GKO. In the experiment it is found that the transmitted signals above about 2 kOe consist of a single sense of circular polarization, whereas the driving field is linearly polarized. The simple theory, which omits discussion of the self-consistent fields at the surface of the sample, does not provide any convincing explanation for this effect.

In the case of thin samples the spectrum is dominated by the resonant bursts of transmission which we have called "cyclotron phase resonance." It is shown that these resonances are not associated with Azbel-Kaner cyclotron resonance, but result from the synchronization of microwave phase, on arrival at the second surface, of electrons on various orbits on the Fermi surface which have the same cyclotron frequency. The resonances are thus associated with regions of Fermi surface with approximately flat mass (as a function of k_H). The theory presented here can account for the phase dependence of these signals, but can only qualitatively reproduce the line shape. Also there is a certain discrepancy in the mass values of the resonances. For {100} copper the experimental mass is about 2% lower than that obtained from the theory in conjunction with the Fermi-surface data of Halse, and about 1% lower for silver. In the case of copper this discrepancy is somewhat greater than the experimental error. Once again the theoretical assumptions concerning the treatment of the surface fields no doubt play a role in the detailed line shapes, as do deviations from flatness in the sample surfaces arising from technical difficulties in preparation.

ACKNOWLEDGMENT

The authors wish to acknowledge the technical assistance of R. E. Miller.

[1]E. A. Kaner and V. F. Gantmakher, Usp. Fiz. Nauk 94, 193 (1968) [Sov. Phys. Usp. 11, 81 (1968)].
[2]W. M. Walsh, Jr. and P. M. Platzman, Phys. Rev. Letters 15, 784 (1965).
[3]R. B. Lewis and T. R. Carver, Phys. Rev. Letters 12, 693 (1964).
[4]S. Schultz and G. Dunifer, Phys. Rev. Letters 18, 283 (1967).
[5]N. S. VanderVen, Phys. Rev. Letters 18, 277 (1967).
[6]G. A. Baraff and T. G. Phillips, Phys. Rev. Letters 24, 1428 (1970).
[7]T. G. Phillips, G. A. Baraff, and P. H. Schmidt, Phys. Rev. Letters 25, 930 (1970).
[8]V. F. Gantmakher and E. A. Kaner, Zh. Eksperim. i Teor. Fiz. 48, 1572 (1965) [Sov. Phys. JETP 21, 1053 (1965)].
[9]V. P. Naberezhnykh and N. K. Dan'shin, Zh. Eksperim. i Teor. Fiz. 56, 1223 (1969) [Sov. Phys. JETP 29, 658 (1969)].
[10]G. Weisbuch and A. Libchaber, Phys. Rev. Letters 19, 498 (1967).
[11]M. R. Halse, Phil. Trans. Roy. Soc. London A265, 507 (1969).
[12]G. E. H. Reuter and E. H. Sondheimer, Proc. Roy. Soc. (London) A195, 336 (1948).
[13]P. M. Platzman and S. J. Buchsbaum, Phys. Rev. 132, 1 (1963).
[14]G. A. Baraff, Phys. Rev. 167, 625 (1968).
[15]D. S. Falk, Phys. Rev. B 3, 1973 (1971).
[16]J. F. Carolan and A. P. van Gelder, Phys. Rev. Letters 25, 1433 (1970).
[17]A. W. Overhauser and S. Rodriguez, Phys. Rev. 141, A431 (1966).
[18]R. B. Lewis and T. R. Carver, Phys. Rev. 155, 309 (1967).
[19]S. Schultz and G. L. Dunifer (unpublished).
[20]M. A. Kinch and B. V. Rollin, Brit. J. Appl. Phys. 14, 672 (1963).
[21]S. Schultz and C. Latham, Phys. Rev. Letters 15, 145 (1965).
[22]The alkali metals appear not to show this behavior [G. L. Dunifer (private communication)].
[23]L. T. Wood and J. D. Gavenda, Phys. Rev. B 3, 1492 (1970).
[24]J. F. Koch, R. A. Stradling, and A. F. Kip, Phys. Rev. 133, A240 (1964).
[25]B. Perrin, G. Weisbuch, and A. Libchaber, Phys. Rev. B 1, 1501 (1970).

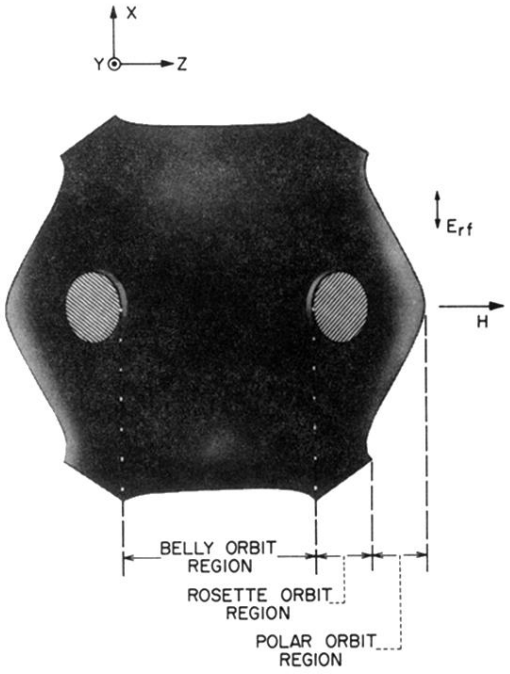

FIG. 2. Typical Fermi surface for a noble metal with H along a $\langle 100 \rangle$ direction, indicating three regions of different orbit types.